Iranian Journal of Catalysis 5(2), 2015, 135-141

IRANIAN JOURNAL OF CATALYSIS

Optical and photocatalytic properties undoped and Mn-doped ZnO nanoparticles synthesized by hydrothermal method: Effect of annealing temperature

Maryam Bordbar[a,*], Seyed Mohammad Vasegh[b], Somaye Jafari[c], Ali Yeganeh Faal[c]

[a]*Department of Chemistry, Faculty of Science, University of Qom, Qom, Iran.*
[b]*Faculty of Technical & Engineering, Islamic Azad University, Tehran South Branch, Tehran, Iran.*
[c]*Faculty of Science, Payame Noor University, Qom, Iran.*

Received 1 September 2014; received in revised form 2 October 2014; accepted 23 October 2014

ABSTRACT

Undoped and Mn-doped ZnO nanoparticles were successfully prepared by the hydrothermal method with different annealing temperature conditions. Structural, chemical and optical properties of the samples were studied by X-ray diffraction (XRD), field emission scanning electron microscopy (FE-SEM), UV-Vis spectrophotometry and Fourier transform infrared (FT-IR) spectroscopy. The phase purity was confirmed by X-ray powder diffraction (XRD) indicating hexagonal wurtzite structure for all samples and less crystallinity with increasing annealing temperature. In addition, the average particle size was found to be 15-30 nm from SEM and XRD. It is seen that the optical band gap increases when the ZnO is doped with manganese and decreases when annealing temperature increases. The photocatalytic activity of undoped and Mn-doped ZnO nanoparticles was tested by the degradation of methyl orang (MO) under UV light and indicated that Mn-doped ZnO has higher photocatalytic activity relative to ZnO nanoparticles and photocatalytic activity decreases when annealing temperature increases.

***Keywords**: Mn-doped ZnO; Photocatalyst; Hydrothermal method; Annealing temperature.*

1. Introduction

The fast moving developments in the field of nanoscience have stimulated considerable research efforts on the synthesis and manufacturing of novel devices for various high-technological potential applications. It has been observed that the various properties of materials such as, electrical, chemical, optical, mechanical properties, etc at nano-level are totally different from their bulk counter parts [1]. The semiconductor nanostructures exhibit themselves as one of the important class, because of the variety of applications such as electronics, optoelectronics sensors and actuators and even in biological systems. Recently, among the metal-oxide photocatalysts, ZnO semiconductor nanostructure have become a focus of attention due to their possible application in electronics, optics, photonics, sensors, transducers, catalyst and to degradation of environmental organic pollutants [2-5].

*Corresponding author email: m.bordbare@gmail.com
Tel.: +98 25 3210 3792; Fax: +98 25 3285 0953

The major advantages of ZnO are a low price, good gas sensing properties, photocatalytic activity, antibacterial activity, possibility to prepare structures with interesting optical properties like photonic crystals, catalytic materials, etc. However, ZnO has almost the same band gap (3.2 ev) as TiO_2, but it is more efficient catalyst because it has more numbers of active sites with high surface reactivity and then generates H_2O_2 more efficiently [6] that resulting higher reaction and mineralization rates than TiO_2 [7,8].

ZnO have been doped whit transitional metal ions such as Co, Sb, Ni, Mn and Fe [9-12] due to that, doping of metal oxide with metal and/or transition metals increases the surface defects [13], which improve the photocatalytic activity. Defects in crystals create energy states within the band gap which act as intermediate steps for electrons in their transitions between the valence and conduction bands as a result of photo excitation [12,14]. However, it is still challenging to major problem is that the defects are interacting with many other factors and the

photocatalytic activity is dominated by the balance among all these factors [15]. It should be mentioned that that defects exist in most ZnO samples except perfect single crystals, and the degree of defects may differ a lot in different samples.

Impurification of ZnO with transitional metal ions as Mn^{2+} is one of the efforts has been improved the photocatalytic activity of ZnO [16-20]. Many factors such as precursor concentration, reaction and temperature time, annealing temperature etc. can be affected crystalline phase and size, electronic structure and crystal defects and then can be affected photocatalytic activity. However, the change of structural characteristics of ZnO nanoparticles under annealing is very complex. It seems that the properties of ZnO nanoparticles could not be ascribed to the size effect or surface chemical compositions singly. The effect of annealing on the properties of ZnO should include the interaction role of different kinds of structural characteristics. Wang et al. reported effect of annealing temperature on the microstructures and photocatalytic property of colloidal ZnO nanoparticles [21]. However, the study of annealing temperature effect on the structural and photocatalytic property of Mn-doped ZnO has not been systematically investigated yet. Herein, we report a simple hydrothermal procedure for the successful fabrication of Mn-doped ZnO nanoparticles with different synthesis annealing temperatures as well as structural and photocatalytic property of Mn-doped ZnO. The work is to study the effects of annealing temperature on the structural and photocatalytic properties of Mn-doped ZnO.

2. Experimental

2.1. Synthesis procedure

The synthesis of undoped ZnO and Mn-doped ZnO nanoparticles was done by facile hydrothermal process. All the chemical reagents used in this work were of analytical grade and used as received without further purification including deionized water, ethanol, zinc acetate dihydrate ($Zn(Ac)_2.2H_2O$), hexamethylene tetramine (HMTA). The dopant source of manganese was manganese nitrate dihydrate ($Mn(NO_3)_2.2H_2O$). The typical procedure for the preparation of undoped ZnO and Mn-doped ZnO nanoparticles was as follows: 25 ml of 0.2 M $Zn(Ac)_2.2H_2O$ aqueous solution with 25 mL of 0.008 M $Mn(NO_3)_2.2H_2O$ (4% mol of $Mn(NO_3)_2.2H2O$) was mixed and stirred at room temperature for 5 min. Then 25 mL of 0.2 M HMTA aqueous solution was added in under stirring condition at room temperature. The mixed solution was magnetically stirred for 30 min and then transferred into Teflon-lined stainless steel autoclave, sealed and heated at 95°C for 20 h. The as-formed precipitates were filtrated and washed with deionized water and ethanol and dried at 60°C in air for further characterization. Finally, the powder was divided to three parts and each was annealed at air for 1h at 300°C, 500°C and 600°C, respectively.

2.2. Characterization

The ZnO samples structure were characterized by X-ray diffraction pattern recorded on a Philips model X'PertPro diffractometer employing Cu Kα radiation (λ=1.5418Å) while the general morphologies of the synthesized samples were investigated by field emission scanning electron microscopy (FESEM;TESCAN-MIRA3) equipped with an Oxford Inca Energy Dispersive X-ray detector. Fourier transform infrared (FT-IR) spectra were obtained using the FT-IR (Jasco, 4200) with the KBr method. UV-Vis spectra were recorded by using a Shimadzu UV-2500 spectrophotometer in the wavelength range 200-700 nm. The photocatalytic property, i.e. Methyl Orange (MO) degradation was evaluated as follows: 10 mg of the samples was dispersed in 50 mL of 0.02 mM methyl orange solution. Before the illumination, the suspensions were magnetically stirred in the dark for 1 h to ensure the establishment of absorption equilibrium of methyl orange on the sample surfaces. After that, suspension was irradiated under a 50 W low-pressure Hg lamp. UV–Vis absorption spectra were recorded at different time to calculation MO concentration.

3. Results and discussion

3.1. Structural properties

The XRD patterns of ZnO and Mn-doped ZnO with annealing temperature at 300°C are shown in Fig. 1. The XRD patterns reveal that samples have a hexagonal structure compared to 79-0206 ASTM card. No diffraction peaks from impurity phases like Zn or MnO_2 were detected, indicating that the resulting sample has only one hexagonal-wurtzite ZnO phase. XRD patterns of undoped ZnO and Mn-doped ZnO show narrow and sharp diffraction peaks, indicating good crystallinity of the synthesized samples. Compared to undoped ZnO, no obvious difference is observed for Mn-doped ZnO, except a slight shift of XRD peaks to a lower angle. Correspondingly, the crystal lattice constants of the nanorods arrays increased in Mn-doped ZnO relative to undoped ZnO, as shown in the Fig. 1b and Table 1. This may be because the radius of Mn^{2+} ions (0.80 Å) is larger than the Zn^{2+} ions (0.74 Å) and correspondingly the c-axis lattice constant increases. It can be seen that with the increasing of temperature annealing, locations of the measured diffraction peaks do not change significantly but the relatively intensity of diffraction peaks decrease obviously, which might be due to the increase in the lattice disorder and strain induced by Mn^{2+} substitution [22].

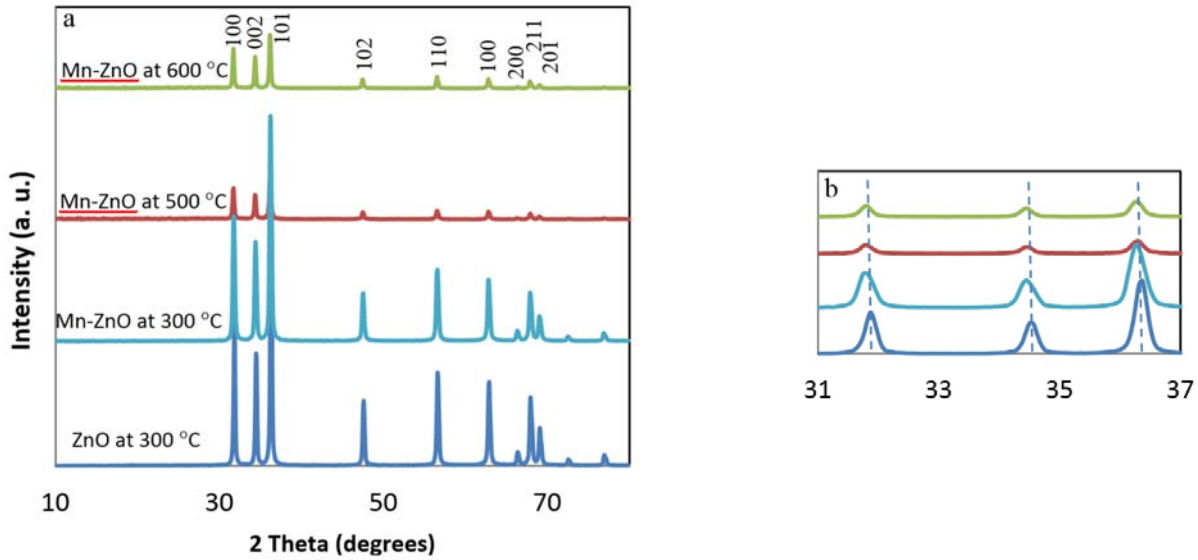

Fig. 1. (a) XRD spectrum of undoped ZnO and Mn-doped ZnO at 300, 500 and 600°C, (b) (100), (002) and (101) Peak position shifting.

With the increase of annealing temperature, atoms obtain more energy to move, and more active incorporation of Mn atoms may do damage to the lattice structure of ZnO, and the enhancement of defects of ZnO in samples.

The lattice constants for undoped ZnO and Mn-doped ZnO with different concentrations are found by using the following equation [18].

$$\frac{1}{d^2} = \frac{4}{3}\left(\frac{h^2+hk+k^2}{a^2}\right) + \frac{l^2}{c^2} \quad (1)$$

The calculated lattice constants are listed in Table 1. The calculated lattice constants of Mn-doped ZnO are different from them in ZnO, suggests the substitution of Mn for Zn in the lattice, also by interstitial zinc atoms or oxygen vacancies. When annealing temperature increases, the lattice constant also increases slightly, that supported with decreasing of intensities of peaks in XRD patterns.

The mean crystallite size was calculated using the Scherrer formula [23]:

$$D = k\lambda/\beta\cos\theta \quad (2)$$

Where λ is the wavelength of X-ray radiation, K is usually 0.89 is the Scherrer constant, λ = 1.54056 Å is the wavelength of the X-ray radiation, β is the peak full width at half maximum in radians and θ is the Bragg diffraction angle. The estimated values of grain size are in 20-30 nm range. The results are summarizes in Table 1.

Fig. 2. displays the SEM images of the synthesized undoped and Mn-doped ZnO at 300°C. This image reveals that the samples have size of 30-50 nm. The energy Dispersive X-ray spectroscopy (EDAX) analysis (Fig. 3) manifests that the sample are composed of Zn, Mn and O.

Fig. 4 shows the FT-IR spectrums of the undoped and Mn-doped ZnO (Mn-ZnO). The strong peaks at 450-500 cm^{-1} corresponds to Zn-O stretching vibration. The broad absorption band observed at ~3428 cm^{-1} corresponds to the O-H stretching vibrations of water present in ZnO. The band at ~1645 cm^{-1} can be associated with the bending vibrations of H_2O molecules. The absorption bands at ~1579 cm^{-1} and ~1425 cm^{-1} in the samples are due to the the C=O and

Table 1. Peak position, grain sizes and lattice constants of undoped and Mn-doped ZnO.

	ZnO	Mn-ZnO		
	300°C	300°C	500°C	600°C
(101) Peak position (degree)	36.3918	36.3243	36.2902	36.2763
Average grain size (nm)	24.4	21.6	26.9	26.7
$a_{(100)}$	3.2345	3.2435	3.2481	3.2486
$c_{(002)}$	5.1842	5.1962	5.2038	5.2051

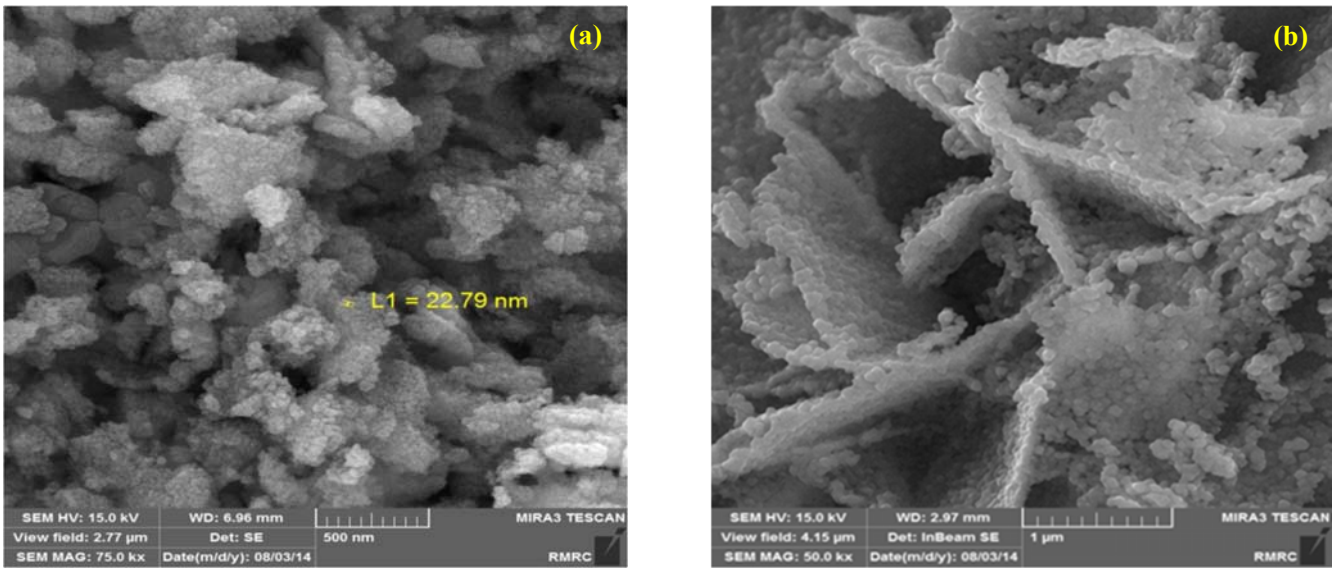

Fig. 2. FE-SEM images of (a) undoped ZnO and (b) Mn-doped ZnO at 300°C.

C-O stretching band for the acetate groups which might remain adsorbed on the surface of ZnO [24]. Also the peak at 1725 cm^{-1} is assigned to asymmetric COO- stretching vibration modes of acetate group [25].

3.2. Optical properties

The UV–Vis absorption spectra of syntesized undoped ZnO and Mn-doped Zn at different annealing temperature are shown in Fig. 5a. All absorption curves exhibit an intensive absorption in 200-380 nm wavelength range, with the absorption edge between 300-370 nm, owing to the relatively large exciton binding energy. These findings are agree well with those obtained by Senthilkumaar et al. [26].

The band gap energy of nanostructures were calculated from $(\alpha h\nu)^2$ vs. hν plot, where α is the optical absorption coefficient from the absorption data and hν is the energy of incident photon. The band gap energy (E_g) was estimated by assuming a direct transition between valence and conduction bands from the following expression [27]:

$$\alpha h\nu = K(h\nu - E_g)^{1/2} \quad (2)$$

Where, K is a constant. The intercepts of these plots afford an estimate of the optical band gap energy of the corresponding samples as shown in Fig. 5b. The wavelengths of maximum absorbance and band gaps for each nanostructure sample are listed in Table 2. Band gap value of 3.00 eV is obtained for undoped ZnO nanostructure while the band gap of Mn-doped ZnO nanostructure sample was found to increases and decrease upon increasing annealing temperature as presented in Table 2. It can be observed, that the band gap (E_g) of ZnO can be tuned over a large energy range using the different annealing temperature.

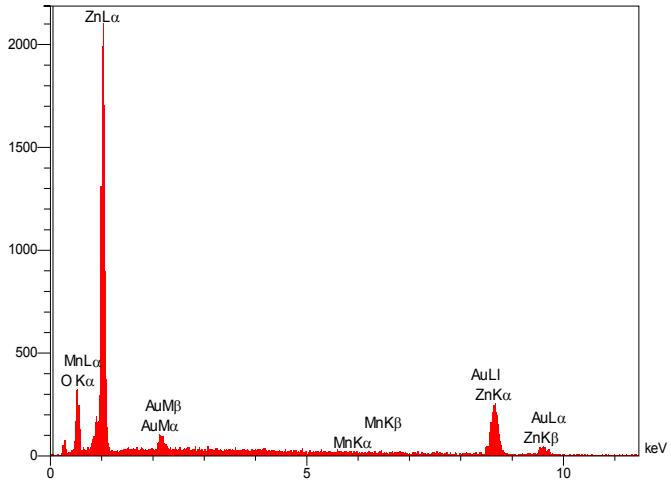

Fig. 3. EDAX analysis of Mn-doped ZnO at 300°C.

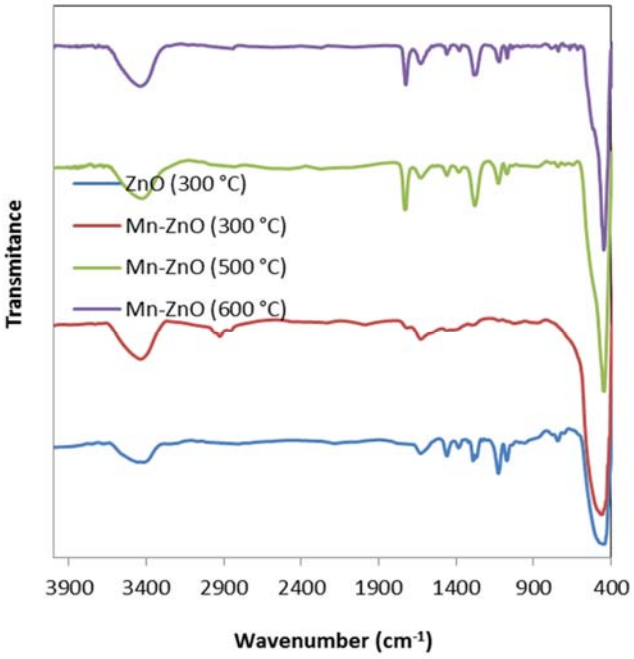

Fig. 4. FT-IR spectra of undoped ZnO and Mn-doped ZnO for 300, 500 and 600°C temperature annealing.

The absorption edge shifts towards higher energy when the Mn is doped in ZnO structure due to Burstein-Moss effect and shifts to lower energy when annealing temperature increases. Although Mn doping is mostly reported to introduce defect states close to the conduction band, it may however narrow the band gap by introducing tail states close to the valence band of ZnO [13], but high Mn doping level (4%) may also increase the band gap of ZnO [28] due to the Burstein–Moss effect [29]. According to the Burstein-Moss shift, at Mn doping, the Fermi level shifts into the conduction band. This results in the absorption transition from valence band to the Fermi level in the conduction band, instead of from the valence band to the bottom of the conduction band due to the donor electron filling of the conduction band [30].

3.3. Photocatalytic experiments

Methyl orang (Scheme 1) is a dye having azo group and sulphonate (SO_3^-) showing an absorption peak at 460 nm. Photodegradation experiments were carried out under UV light and in aqueous solution in the presence of different synthesized samples. The changes in the UV-Vis spectra of MO (0.02 mM) under UV irradiation in the presence of Mn-doped ZnO (0.2 g/L) are shown in Fig. 6(a).

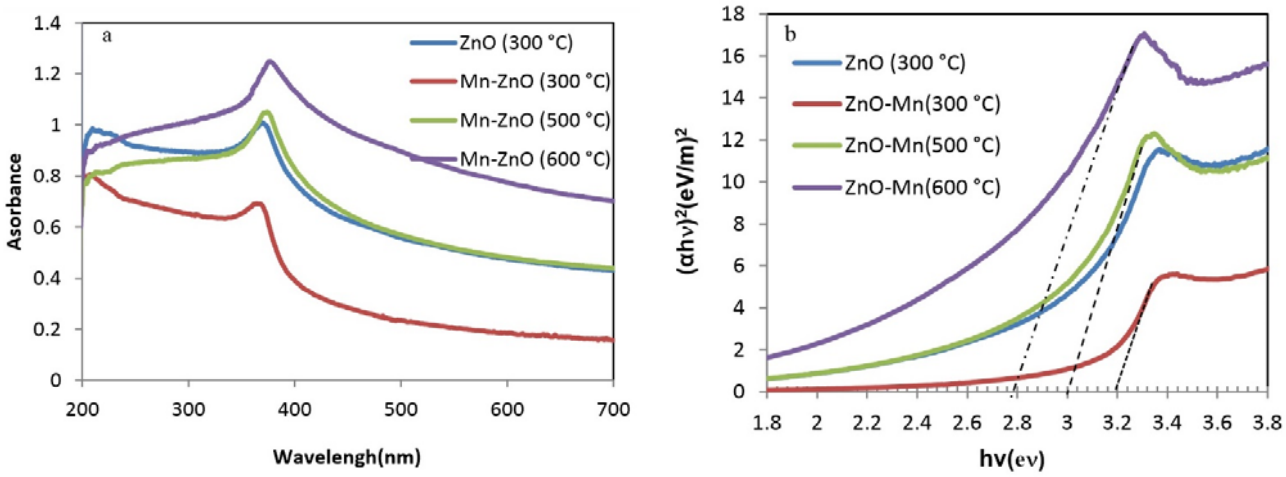

Fig 5. (a) UV-Vis spectrum of undoped and Mn-doped ZnO and for different annealing temperature (300, 500 and 600°C); (b) corresponding $(\alpha h\nu)^2$ vs $h\nu$ plots.

Table 2. Band gap energy and the excitation, Maximum wavelength data and photo-degradation rate constant of samples.

	ZnO	Mn-ZnO		
	300°C	300°C	500°C	600°C
Wavelength (nm)	367.5	364.0	374.0	376.5
Band gap (eV)	3.00	3.16	2.96	2.70
k (min^{-1})	0.0059	0.0075	0.0043	0.0039

As it is presented in Fig. 6(a), the bands relating to different molecular parts in this dye are decreased with respect to time. The disappearance of the 460 nm absorption band, suggests that the chromophore part of molecular structure is breaking down. A part from the degradation of the colored group, the decrease of the absorbance values at the UV region, is ascribed to the •OH radical attack and breaking of the aromatic rings in the dye molecule.

Results of the photocatalytic tests of synthesized sample, given in Fig. 7(b) and Table 2, show that the degradation followed first order kinetics as per Eq. (3).

$$ln\left(\frac{C}{C_0}\right) = -kt + B \qquad (3)$$

Where C_0 represents the initial MO concentration, C stands for its concentration at any time t of the photo-irradiation, and k is the apparent degradation rate constant. It can been seen that the degradation rate constant (k = 0.0075 min^{-1}) of synthesised Mn-doped ZnO catalysts at 300°C annealing temperature is higher than the others. Actually, the photocatalytic activity increases from undoped ZnO to Mn-doped ZnO at 300°C and decreases when annealing temperature increases. These data support the results found for band gap energies that are higher for Mn-doped ZnO at 300°C comparison with others, because of UV output irradiation of the Hg lamp.

As the UV light falls on the ZnO, the valence band electron of ZnO jumps to the conduction band leaving behind a void or positively charged hole [11]. It is well known that three factors contribute to the enhancement of the photocatalytic activity: increasing the surface active sites, modifying the band of the semiconductor, and hindering the recombination of photogenerated electrons and holes [31]. The lattice defects such as oxygen vacancy could serve as favorable trap sites of the electrons or holes to reduce their recombination and consequently increase the photocatalytic activities [32].

As it listed in Table 2, the synthesized Mn-doped ZnO (300°C) catalysts has the highest photocatalytic degradation percentage compare with the other samples, because of any or both of the two obvious reasons.

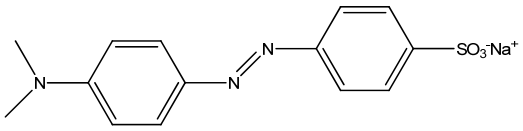

Scheme 1. Methyl Orange Structure.

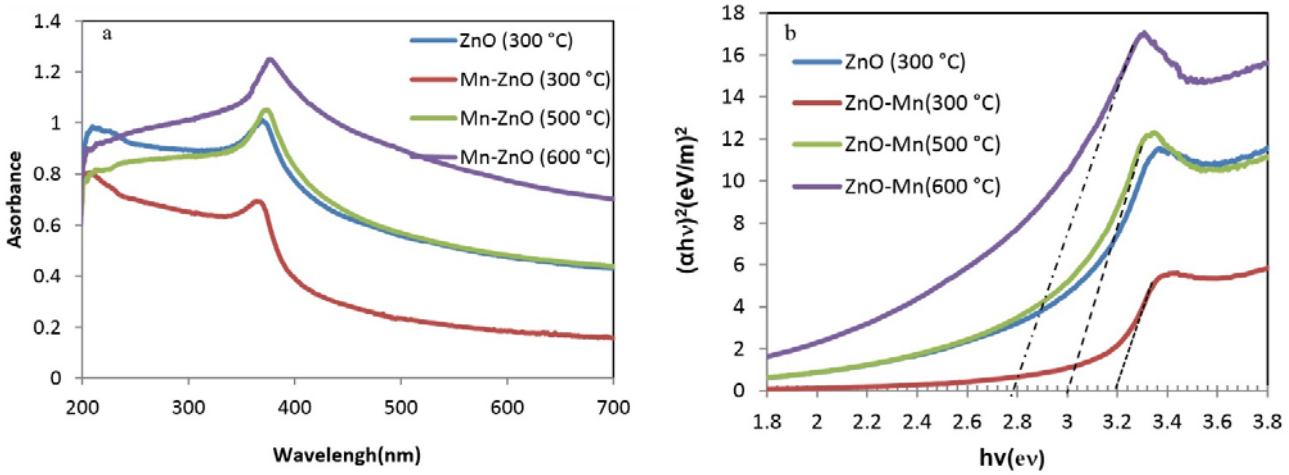

Fig 6. (a) Photodegradation of methyl orange (MO) using the Mn-doped ZnO at 300°C (b) the relationship between C/C_0 and reaction time.

One is the comparatively large surface area and more active sites which is related to the smaller crystal of the photocatalyst sample (Table 1). Therefore, much more space is available for the absorption of methyl orange, and the improvement of photocatalytic degradation percentage is inevitable; the other is the increased band gap and increasing absorption the ultraviolet light irradiation of high pressure mercury lamp. We can conclude that annealing temperature has high effect on the photocatalytic activity of Mn-doped ZnO. The development of such photocatalysts for remediation of water polluted investigates of effect of annealing temperature, as a synthesis parameter could be useful.

4. Conclusions

Zinc oxide nanoparticles doped with manganese were synthesized by a hydrothermal method and were used as a catalyst in the process of photodegradation of methyl orange as a dye model. Doping of ZnO with manganese results in an enhanced photodegradation efficiency. Based on the experimental results obtained in this study, the photodegradation efficiency was influenced by different reaction parameters such as the existence of dopant and annealing temperature. The absorption edge shifts to longer wavelengths with the increase of annealing temperature. The maximum photodegradation efficiency for methyl orange was obtained with a catalyst Mn-ZnO with annealing temperature at 300°C. The enhanced

photocatalytic activity of Mn-doped ZnO might be ascribed to the increase of surface-to-volume ratio, mean grain size, oxygen defects density and increase band gap relative to undoped ZnO.

Acknowledgments

This work was supported by Payam Noor University and University of Qom.

References

[1] A. Umar, Y.B. Hahn, Metal oxide nanostructures and their applications, American Scientific Publication, 2010.
[2] O.I. Lupan, S.T. Shishiyanu, T.S. Shishiyanu, Superlattices Microstruct. 42 (2007) 375-378.
[3] J. Guo, J. Zhang, M. Zhu, D. Ju, H. Xu, B. Cao, Sens. Actuators B: Chem. 199 (2014) 339-345.
[4] R. Khan, M.S. Hassan, L.W. Jang, J.H. Yun, H.K. Ahn, M.S. Khil, I.H. Lee, Ceram. Int. 40 (2014) 14827-14831.
[5] Y. Chen, D. Bagnall, T. Yao, Mater. Sci. Eng. B 75 (2000) 190-198.
[6] E.R. Carraway, A.J. Hoffman, M.R. Hoffmann, Environ. Sci. Technol. 28 (1994) 786-793.
[7] I. Poulios, D. Makri, X. Prohaska, Global Nest: Int. J. 1 (1999) 55-62.
[8] B. Pal, M. Sharon, Mater. Chem. Phys. 76 (2002) 82-87.
[9] R.Y. Hong, S.Z. Zhang, G.Q. Di, H.Z. Li, Y. Zheng, J. Ding, D.G. Wei, Mater. Res. Bull. 43 (2008) 2457-2468.
[10] C. Xu, L. Cao, G. Su, W. Liu, X. Qu, Y. Yu, J. Alloys Compd. 497 (2010) 373-376.
[11] C. Wu, L. Shen, H. Yu, Q. Huang, Y.C. Zhang, Mater. Res. Bull. 46 (2011) 1107-1112.
[12] S. Yılmaz, E. McGlynn, E. Bacaksız, J. Cullen, R.K. Chellappan, Chem. Phys. Lett. 525–526 (2012) 72-76.
[13] R. Ullah, J. Dutta, J. Hazard. Mater. 156 (2008) 194-200.
[14] M.A. Mahmood, S. Baruah, J. Dutta, Mater. Chem. Phys. 130 (2011) 531-535.
[15] X. Zhang, J. Qin, Y. Xue, P. Yu, B. Zhang, L. Wang, R. Liu, Sci. Rep. 4 (2014).
[16] Y.L. Chen, C.E. Zhang, C. Deng, P. Fei, M. Zhong, B.T. Su, Chin. Chem. Lett. 24 (2013) 518-520.
[17] L. Shi, L. Liang, J. Ma, J. Sun, Superlattices Microstruct. 62 (2013) 128-139.
[18] J.B. Zhong, J.Z. Li, X.Y. He, J. Zeng, Y. Lu, W. Hu, K. Lin, Curr. Appl. Phys. 12 (2012) 998-1001.
[19] M. Ahmad, E. Ahmed, Z.L. Hong, X.L. Jiao, T. Abbas, N.R. Khalid, Appl. Surf. Sci. B. 285 (2013) 702-712.
[20] J.C. Sin, S.-M. Lam, I. Satoshi, K.T. Lee, A.R. Mohamed, Appl. Catal. B: Environ. 148–149 (2014) 258-268.
[21] H. Wang, C. Xie, J. Phys. Chem. Solids 69 (2008) 2440–2444.
[22] K. Omri, J. El Ghoul, O.M. Lemine, M. Bououdina, B. Zhang, L. El Mir, Superlattices Microstruct. 60 (2013) 139-147.
[23] A. Patterson, Phys. Rev. 56 (1939) 978.
[24] R. Saravanan, V.K. Gupta, V. Narayanan, A. Stephen, J. Mol. Liq. 181 (2013) 133-141.
[25] K. Kaviyarasu, P.A. Devarajan, Adv.Mat. Lett. 4 (2013) 582-585.
[26] S. Senthilkumaar, K. Rajendran, S. Banerjee, T.K. Chini, V. Sengodan, Mater. Sci. Semicond. Process 11 (2008) 6-12.
[27] L. Brus, J. Phys. Chem. 90 (1986) 2555-2560.
[28] Y.S. Wang, P.J. Thomas, P. O'Brien, J. Phys. Chem. B. 110 (2006) 21412-21415.
[29] Z. Banu Bahşi, A.Y. Oral, Opt. Mater. 29 (2007) 672-678.
[30] N.S. Sabri, A.K. Yahya, M.K. Talari, J. Lumin. 132 (2012) 1735-1739.
[31] M. Wen, M. Cheng, S. Zhou, Q. Wu, N. Wang, L. Zhou, J. Phys. Chem. C. 116 (2012) 11702-11708.
[32] S. Yamamoto, H. Watarai, J. Phys. Chem. C. 112 (2008) 12417-12424.